energies

MDPI

Article

Validation of Actuator Line and Vortex Models Using Normal Forces Measurements of a Straight-Bladed Vertical Axis Wind Turbine

Victor Mendoza * and Anders Goude

Division of Electricity, Department of Engineering Sciences, Uppsala University, P.O. Box 534, 751 21 Uppsala, Sweden; anders.goude@angstrom.uu.se

* Correspondence: victor.mendoza@angstrom.uu.se; Tel.: +46-18-471-5843

Received: 13 November 2019; Accepted: 16 January 2020; Published: 21 January 2020

Abstract: Vertical Axis Wind Turbines (VAWTs) are characterized by complex and unsteady flow patterns resulting in considerable challenges for both numerical simulations and measurements describing the phenomena involved. In this study, a 3D Actuator Line Model (ALM) is compared to a 2D and a 3D Vortex Model, and they are validated using the normal forces measurements on a blade of an operating 12 kW VAWT, which is located in an open site in the north of Uppsala, Sweden. First, the coefficient power (C_P) curve of the device has been simulated and compared against the experimental one. Then, a wide range of operational conditions for different tip speed ratios (TSRs), with λ = 1.84, 2.55, 3.06, 3.44, 4.09 and 4.57 were investigated. The results showed descent agreement with the experimental data for both models in terms of the trend and magnitudes. On one side, a slight improvement for representing the normal forces was achieved by the ALM, while the vortex code performs better in the simulation of the C_P curve. Similarities and discrepancies between numerical and experimental results are discussed.

Keywords: vertical axis wind turbines; actuator line model; vortex method; dynamic stall model

1. Introduction

A renewed interest in VAWTs has arisen from the current trend of wind energy industry aiming for large scale turbines in offshore farms [1–3]. VAWTs offer a potential reduction in the total energy production cost over the conventional Horizontal Axis Wind Turbines (HAWTs). In Reference [4], Musgrove claimed that VAWTs can be made substantially larger than HAWTs. HAWTs have a limiting factor for upscaling, since gravity produces tension-compression cycles (fatigue) on the blades as the rotor rotates [5], while VAWTs do not undergo this phenomenon and can be produced taking advantage of significant economies of scale [6]. Additionally, the omni-directionality of VAWTs allow them to operate with incoming wind from any direction, this also simplifies the mechanical design using a few moving parts without a yawing system and often excluding the pitching system. This is a relevant characteristic since a considerable part of failures on the HAWTs occurs in the yawing mechanism: Ribrant and Bertling [7] showed that for a typical HAWT in Sweden, the failure in the yawing systems represents the 13.3% of the total mean downtime per year. In Reference [8], Tavner et al. claimed that the principal contributors to the higher failure rate on German wind turbines are electrical control or system sub-assemblies (i.e., yawing). Arabian-Hoseynabadi et al. [9] scored the yawing system with a risk priority number (RPN) of 813, ranking it on the seventh place among the other assemblies. Another considerable advantage of VAWTs is that the generator can be located at the sea level, improving the stability of the structure and additionally reducing the size and cost of the floating fundation. Therefore, concerns about dimension and weight of the generator are minimized, allowing

the installation of heavy direct driven generators using permanent magnets [10]. When it comes to operation and maintenance costs on offshore environment, which are estimated to be comparable to the cost of the wind turbine itself, it is difficult and expensive to replace large components at sea when you have to work on a platform that can move. In the case of VAWTs, the machinery can be easily accessed. All these VAWTs potentials for scalability are being studied by both European and American research programs [1,11].

VAWTs are characterized by complex and unsteady three-dimensional fluid dynamics. VAWT blades are inherently exposed to cyclic variation in the angle of attack producing cyclic forces which are a potential source for damage due to fatigue. The blade's circulation around the rotation axis of the turbine produces a different wake compared to the produced by a HAWT. The near-wake structure is mainly characterized by the vortical structures released by the blade tips and the blade pitching motion. This creates recovery levels due to the vertical flow advection which is larger than the one produced by the turbulent fluctuations [12]. This effect does not happen for HAWTs, in which the wake is only generated by tip vortices. In a VAWT with fixed pitch, the angle of attack is oscillating and its amplitude is increasing with decreased tip speed ratio (TSR). At low TSR, the blades usually will experience dynamic stall, where the blade force coefficients are not only dependent of the angle of attack but also of its rate of change.

In order to understand and predict the loads on blades of operational VAWTs for their design, it is fundamental to have both experimental data and reliable numerical tools. Unfortunately, there is not a considerable amount of experimental results for forces on blades for VAWTs. During the 80's, Sandia National Laboratories carried out some experimental works on VAWTs of the Darrieus type (with curved blades) at open sites—in Reference [13], field test data were gathered on numerous characteristics of VAWT operation using systems with 17, 5 and 2 meters of diameter, installed at the Sandia test site. In Reference [14], measurements of surface pressures on a VAWT have been described using pressure transducers mounted at the equator of one blade of the rotor of radius 8.36 m, and which blades have a NACA0015 cross section with a chord of 0.612 m. Oler et al. [15] obtained the instantaneous pressure distributions on a single-bladed rotor operating in a tow tank. There have been additional reports of small VAWT operating at low Reynolds number on wind tunnels and water tanks [16–18].

In the present work, as a main goal, measurements of the C_P curve and aerodynamic normal forces on a 12 kW straight-blade vertical axis wind turbine have been used to validate and evaluate the accuracy of an ALM and a vortex model for simulating the device and to reproduce the forces acting on the blades. The tested turbine is operating at an open site in the north of Uppsala, Sweden [19–21].

2. Theory

In the present study, an actuator line model (ALM) and two vortex models are validated using experimental results of the blade normal forces from a VAWT at an open site for different operating conditions. The focus is on the modeling part of the normal forces acting on the blades within one revolution.

2.1. The Actuator Line Model

The governing equations are solved using an Actuator Line Model (ALM) [22–25], which is based on the blade element theory coupled to a Navier-Stokes solver for the flow field description. First, the ALM samples the flow velocity which gives the angle of attack and relative velocity for each blade element. Then, a Dynamic Stall Model (DSM) determines the blade force coefficients, which the ALM imparts back into the flow solver as body forces. The Large Eddy Simulation (LES) approach is used to predict the turbulence effects. The library turbinesFoam developed by Bachant et al. [26–28] was used for the implementation of the (ALM). This model was previously validated in Mendoza, Bachant et al. [29] and Medoza and Goude [30] using experimental data of

forces on a pitching airfoil within a wind tunnel and normal forces on one blade of an operating turbine at an open site, respectively.

The employed ALM is based on the 3D and unsteady aerodynamic model developed by Sørensen and Shen [31], which is used to study the flow field around wind turbines. The ALM considers the blade as a line of n-elements, which act as 2D aerodynamic profiles. The acting forces are determined using a DSM usually based on empirical data. The implementation of the ALM requires values of the airfoil lift and drag coefficients for different angle of attacks and Reynolds numbers. The relative flow velocity V_{rel} and the angle of attack α are calculated by the geometrical result between the blade rotational velocity $-\Omega r$, with Ω as the angular velocity and r the turbine radius and the local incoming flow $\vec{V}_{\text{in}}$ (which usually has a lower magnitude than the freestream velocity $\vec{V}_{\infty}$). Dynamic stall effects on the force curves were considered using the Leishman-Beddoes DSM [32], including the modifications of Sheng et al. [33] and Dyachuk [34]. The coefficients are obtained using a linear interpolation from a table for a specific angle of attack, therefore by using them together with the blade element approach, the body acting forces can be determined. A diagram of the vectors of velocity and force acting on the cross-sectional airfoil element is depicted in Figure 1.

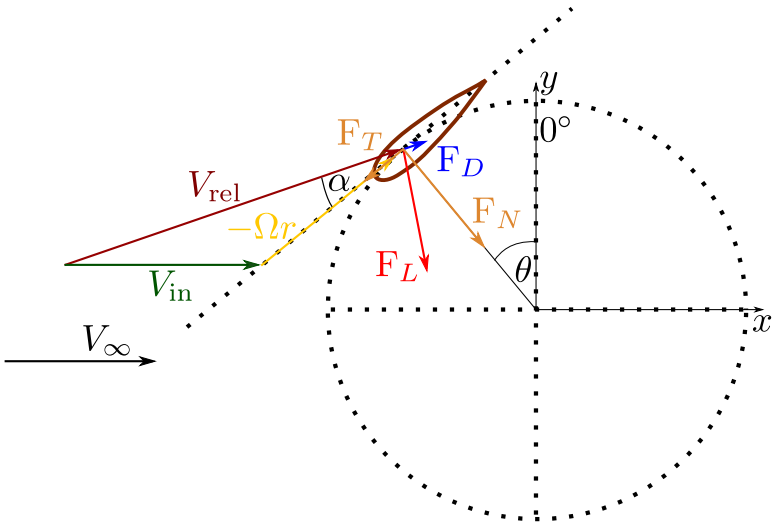

Figure 1. Illustration of velocity vectors and forces acting at the cross-section airfoil element.

Once α and V_{rel} are calculated, the lift and drag forces per spanwise length unit can be obtained as

$$f_L = \frac{1}{2}\,\rho\, c\, C_L\, |V_{\text{rel}}|^2 \tag{1}$$

$$f_D = \frac{1}{2}\,\rho\, c\, C_D\, |V_{\text{rel}}|^2, \tag{2}$$

with C_L and C_D representing the lift and drag coefficients, respectively, both are functions of α and the local Reynolds number. The lift component is orthogonal to V_{rel} and the shaft, while the drag component has the same direction as V_{rel}. The normal force F_N, is the resultant of the aerodynamic force in the radial direction. The tangential force F_T is commonly employed to express the turbine torque during one revolution.

The same procedure is considered to obtain the forces on the turbine shaft and struts. Then, once all the forces in the actuator lines are calculated, they are added a source of body force per unit of density on the momentum conservation (Equation (6)).

In order to avoid numerical instabilities due to large gradients, the applied forces in the ALM are dispersed smoothly on several mesh cells. The source term forces must be projected around the element position employing a three-dimensional Gaussian kernel. The smoothing function η is

employed, which is multiplied by the calculated local force on the actuator line element and imparted on a cell with a distance $|\vec{d}|$ from the quarter chord location of the actuator line element

$$\eta = \frac{1}{\epsilon^3 \pi^{3/2}} \exp\left[-\left(\frac{|\vec{d}|}{\epsilon}\right)^2\right]. \tag{3}$$

The smoothing width parameter ϵ, is chosen by the maximum value of three different contributions related to a quarter of the chord length, the mesh size and the momentum thickness due to drag forces. It can be expressed as

$$\epsilon = \max\left[\frac{c}{4}, 4\sqrt[3]{V_{\text{cell}}}, \frac{cC_D}{2}\right], \tag{4}$$

where V_{cell} represents the volume of the cell.

The local inflow velocity vector, $\vec{V}_{\text{in}}$, is considered as an averaged of the velocity at a number axisymmetric points surrounding the quarter chord position at a defined radial distance. Then, two new factor are introduced to determine the sampling points vector: the number of sampling points and the radial distance between the sampling points location and the quarter chord position. A further study into this approach was carried out, revealing that a suitable combination for the sampling radius and samples number is 2ϵ and 20, respectively.

2.1.1. The Large Eddy Simulation Framework

The Navier-Stokes equations used by the ALM for the involved flow field can be considered for the incompressible case as

$$\frac{\partial \tilde{u}_i}{\partial x_i} = 0 \tag{5}$$

$$\frac{\partial \tilde{u}_i}{\partial t} + \frac{\partial \tilde{u}_i \tilde{u}_j}{\partial x_j} = -\frac{1}{\rho}\frac{\partial \tilde{p}}{\partial x_i} + \nu \frac{\partial^2 \tilde{u}_i}{\partial x_j \partial x_j} - \frac{f_i}{\rho} - \frac{\partial \tau_{ij}}{\partial x_j}, \tag{6}$$

with $\tilde{u}_i$ and $\tilde{p}$ represent the velocity and pressure grid-filtered values, respectively, ν is the kinematic viscosity, f_i the acting body (blade) forces and τ_{ij} corresponds to the sub-grid scale (SGS) stress defined as $\tau_{ij} = \widetilde{u_i u_j} - \tilde{u}_i \tilde{u}_j$.

2.1.2. The Smagorinsky Model

The Smagorinsky model [35] is considered for parameterizing the SGS stress as

$$\tau_{ij} - \frac{1}{3}\delta_{ij}\tau_{kk} = -2(C_S \widetilde{\Delta})^2 |\widetilde{S}| \widetilde{S}_{ij} \tag{7}$$

where $\widetilde{S}_{ij} = \frac{1}{2}\left(\frac{\partial \widetilde{u}_i}{\partial x_j} + \frac{\partial \widetilde{u}_j}{\partial x_i}\right)$ represents the resolved rate-of-strain tensor, $\widetilde{\Delta}$ is the grid size and C_S as the Smagorinsky constant, which usually has the value 0.1 to 0.2. For the present study the used value for this constant is $C_S = 0.1667$, since it is within the range for representing mixing layer flows [36].

2.2. The Vortex Model

The vortex method solutions are based on a similar principle as the ALM, in that it calculates the velocity field, which is then used to obtain the relative flow velocity and the angle of attack which then can be used by a dynamic stall model to calculate the blade forces, which are then included into the flow field. The dynamic stall model used is the same as for the ALM. The two-dimensional vortex model is described in detail in Reference [37] and only a brief description is given here.

The vortex method is based on discretizing the vorticity field instead of the velocity field. The methods used here are free-vortex methods, which means that the vorticity elements are propagated with the flow velocity. The two-dimensional method uses point vortices and the

three-dimensional model uses vortex filaments to describe the flow. A visualization of the filament lattice that is generated from one blade and its support arms in the 3D method is illustrated in Figure 2, where each blade and each support arm will have its own lattice of vortex filaments describing its contribution to the flow field. The flow velocity is obtained by solving Biot-Savart's law at each time-step.

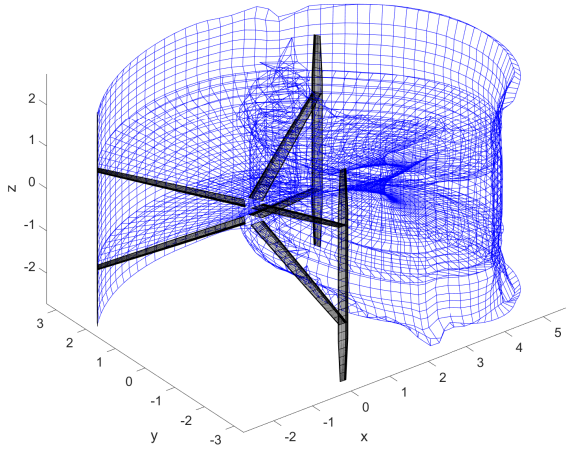

Figure 2. Illustration of filaments from one blade after the first revolution. Each blue line represent one vortex filament in the wake and the black lines represent the filaments used to solve the potential flow for the angle of attack calculation. Each blade will have one of these filament lattices behind them (although only one of them is shown here).

The flow description in the vortex method consists of both the released vortices and a bound vortex that follows each blade. As the forces are calculated through the dynamic stall model, Kutta Joukowski's lift theorem

$$f_L = -\rho V_{rel} \Gamma, \tag{8}$$

where Γ is the bound circulation. See Figure 1 for definition of the relative flow speed. It is assumed that the bound vortex is located at the quarter chord position and V_{in} is sampled at this position to obtain V_{rel}. Note that this will neglect the effect that the drag force has on the wake, which is considered acceptable as the lift force is much larger. The released vortex strength is calculated as the change in bound circulation around the blade, to conserve the total circulation. For the three-dimensional case, the tip vortex strength is automatically obtained when enforcing the divergence free characteristic of the vorticity field.

A significant difference between the ALM implementation and the vortex method implementation is how the angle of attack is calculated. Instead of sampling the velocity at the quarter chord position, a potential flow solution is used. In the two-dimensional case, a linear panel method is used to model the surface of the blade. By solving the no-penetration boundary condition together with the Kutta condition, the circulation of the blade is obtained. The kutta condition is implemented by assuming that the flow behind the trailing edge (evaluated at the distance the blade travels for half a time-step) should be parallel to the blade center line. The dependence between the angle of attack and the circulation was obtained by testing the method for a single blade in steady flow at known angles of attack. This calibration was used to compensate for any static errors possibly introduced by this method of calculating the angle of attack. For the three-dimensional case, a similar procedure was used, but due to the significantly larger number of discretization elements required, the blades were modeled as flat surfaces using a vortex lattice. A validation test was performed in 2D with the linear

panel method exchanged to a line of point vortices as the 2D equivalent of a vortex lattices, and the test showed very good agreement with the linear panel method, indicating that the vortex lattice is a valid approximation. The use of a vortex lattice to solve the no-penetration boundary condition of the flat surface will generate the tip vortices directly, and there is no need for any additional tip correction model with this approach (compared to the ALM). The panel method was only used to calculate the angle of attack. For the vortex convection step, the blades were approximated as individual bound vortices according to the lifting line theory. The reason for this is that due to the use of the dynamic stall model, the circulation obtained from Kutta Joukowski's lift theorem in Equation (8) is lower than the one obtained from solving the Kutta condition. Hence, it is not suitable to use the original panels for the vortex propagation step. This procedure is validated in Reference [38].

In the two-dimensional model, 3D effects were artificially added by applying the correction from Prandlt's finite wing theory and the support arms were added by calculating the drag forces, while the lift generation on the support arms were neglected. See Reference [39] for details. In the three-dimensional model, the support arms were included as additional blade elements, and hence treated equally as the blades (which includes the lift generation on the support arms).

A step by step scheme of a time-step in the vortex method is as follows

1. Calculate the circulation from potential flow solution using the panel method and evaluate the relative flow velocity at the quarter chord position
2. Convert the circulation to an angle of attack using the calibrated lookup table
3. Calculate the circulation from Kutta Joukowski's lift formula
4. Determine the released circulation from the change in circulation add add these vortices to the flow
5. Calculate the flow velocity at each vortex point using Biot-Savart's law and propagate all vortices with the flow speed

The vortex methods used 90 steps per turbine revolution. The three dimensional simulations were performed for 25 turbine revolutions each, while the computationally much cheaper two dimensional simulations were allowed to run 100 revolutions each. In 3D, the blades were modelled by 27 different spanwise segments, while 15 segments were added for each support arm.

3. Simulation Parameters: Validation Case

Experimental data from a 12 kW VAWT, which is shown in Figure 3, was used for validation and evaluation of the reliability and performance of the applied models. The turbine has a diameter of 6.48 m and it is located in an open site in the North of Uppsala (Sweden). The experimental activity for the measurements and obtained forces is available in References [21,22], respectively. Forces on one blade and its struts have been measured using four load cells. Table 1 shows the relevant specifications of the mentioned turbine. The central shaft (tower) and arm struts are considered within the simulation. The details for the struts shape can be found in Reference [40].

Table 1. Specification of the 12 kW Vertical Axis Wind Turbines (VAWT) used for validation.

Number of blades	3
Turbine diameter	6.48 m
Hub height	6.0 m
Blade length	5.0 m
Airfoil profile	NACA0021
Chord length	25 cm
Blade pitch angle	2°
TSR	3.44

Figure 3. The 12 kW turbine, designed and built by the Division of Electricity at Uppsala University. The turbine is equipped with load cells used for the force measurements [21].

For the ALM, the presented turbine was operating such that the freestream velocity V_∞ at the equatorial blade plane (z_∞ = 5.75 m) is defined by using the log law for the different TSRs. Therefore, a logarithmic inlet profile with a non-slip boundary condition for the ground has been tested

$$V_x = \frac{V_{x*}}{K} ln\left(\frac{z + z_0}{z_0}\right), \tag{9}$$

where z_0 represents the roughness length and K = 0.40 is the von Kármán constant. For the present work, z_0 equals to 0.025 m which is a reasonable value for the place where the turbine is located. In the cases using the vortex model, a uniform flow was used.

An important operational parameter for the turbine is the TSR λ, which is defined as the ratio of blade tip speed and the asymptotic freestream flow velocity

$$\lambda = \frac{\Omega r}{V_\infty}, \tag{10}$$

where Ω denotes the rotor angular speed and r the radius of the rotor.

4. Results and Discussion

In this section the calculated power coefficient curve of the turbine and the normal forces on the blade and struts are compared against experimental results, also, similarities and discrepancies between numerical and experimental data are discussed. The turbine power coefficient is defined as

$$C_P = \frac{P}{\frac{1}{2} A \rho V_\infty^3}, \tag{11}$$

with P representing the average power over one revolution, A the projected area of the rotor and ρ the air density. The ALM was tested using the lift and drag coefficients from the report of Sheldahl and Klimas [41] and also from the XFOIL program [42] in order to test the response from the model to different coefficient inputs and its influence on the results accuracy. These two tested versions of the ALM are further denoted as ALM-SK and ALM-XFOIL, respectively. The vortex method was only tested with the data from Sheldahl and Klimas.

4.1. Spatial Sensitivity of the ALM

A test of the sensitivity to the mesh variation has been carried out for the ALM. A reference mesh topology with a uniform hexahedral distribution of cells with a size of 2 m (in every component) was used for this purpose. A local refinement level from n = 1 up to 5 was applied in the region close to the rotor (the base cell is divided into 2^{3n} sub-cells) in order to capture the details of the resulting flow field and to check the response of the model to the spatial variation (further local refinements were not possible due to computational memory restrictions).

An illustration of a local refinement and the obtained power coefficient results for a TSR of $\lambda = 4.02$ using different local refinement levels is depicted in Figure 4. Considering the last two levels of of refinement ($n = 4$ and 5), bigger refinements will not produce a considerable fluctuation (or improvement) on the estimated C_P. The level $n = 4$ has a good agreement with the expected experimental value and hence, it is considered as an acceptable value for the ALM mesh resolution and used in the remaining parts of the study.

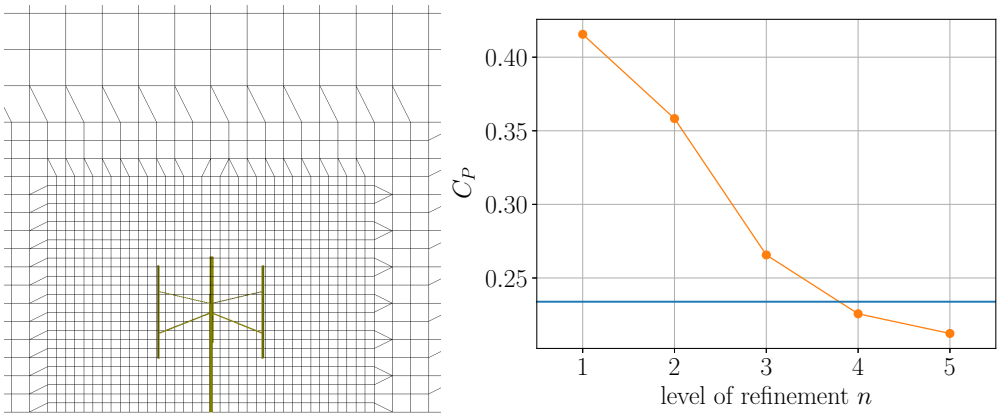

Figure 4. Example illustration of the reference mesh section with a local refinement level of $n = 2$ (**left**) and the power coefficient response at $\lambda = 4.02$ for mesh variation using different level of refinement (**right**). The horizontal blue line represents the experimental value for the tested λ.

4.2. Power Coefficient Curve

The power coefficient curve of the tested turbine $C_P(\lambda)$ has been calculated as function of the TSR. This curve gives information about the aerodynamic properties of the turbine and also it allows to identify the optimal operating TSR. At the time of the experimental activity, which is described and documented in Reference [19], a modified version of the VAWT mentioned above was used without having implemented yet the load cells, and then, the diameter of the turbine rotor was 6 m. Additionally, the blade pitch angle was equal to 0° instead of 2°.

The power curve was simulated using the different models and the results were compared against the experimental data for the different TSRs, as it is revealed in Figure 5. The numerical power curves show descent agreement with the experimental one in terms of the trend and it allows is to identify, at least qualitatively, the region for an optimal TSR operation, which occurs around $\lambda = 3.0$ to $\lambda = 3.7$. There is an evident underestimation of the estimated power by the ALM-SK and, on the other hand, the 2D vortex model overestimated the available power for TSRs bigger than $\lambda = 3$. Table 2 reveals the

standard deviation of the calculated power curves for the different employed models. The ALM-XFOIL and 3D vortex models had the best performance for both representing the experimental values and calculating the maximum C_P value, which is approximately 0.3. All the models differed significantly with experiments for the larger TSRs. The lower performance was achieved by the ALM-SK and 2D vortex models, with a considerable difference for representing the maximum C_P value (around 0.05). Note that the accuracy of the measurements is much lower at high TSRs.

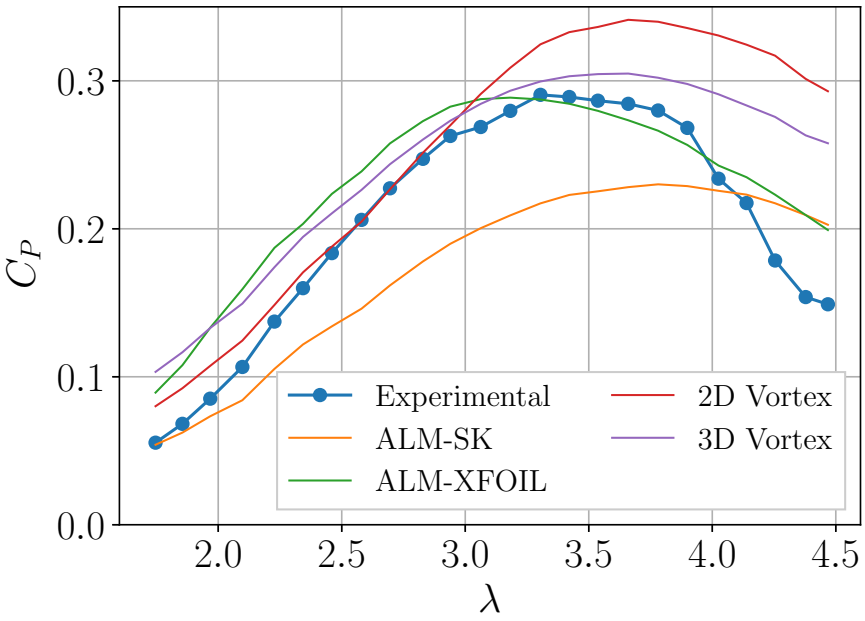

Figure 5. C_P as a function of λ.

Table 2. Standard deviation of the calculated power coefficient C_P as function of λ, for the different employed models.

ALM-SK	ALM-XFOIL	2D Vortex	3D Vortex
0.051984	0.032374	0.062439	0.045534

4.3. Normal Forces

Numerical and experimental results of normal forces on the blades and struts are compared for validating the presented models. These results, have been tested for a wide range of TSRs with λ = 1.84, 2.55, 3.06, 3.44, 4.09 and 4.57 and, therefore, considering from shallow to deep stall operating conditions. Every experimental data set is presented together with their maximum measurement error. The measured normal forces correspond to the averaged values of at least five turbine revolutions.

It has been calculated the standard deviation of the models for all the presented cases (with different TSRs), in Table 3. This, together with the predicted normal forces over one revolution, allows to describe qualitatively and quantitatively the similarities and discrepancies between the calculated and experimental values of the acting normal forces on the blades.

Table 3. Standard deviation of the calculated normal forces for the models at different tip speed ratios (TSRs).

TSR	ALM-SK	ALM-XFOIL	2D Vortex	3D Vortex
1.84	52.4448	52.1865	55.3449	53.1889
2.55	54.9516	70.0141	74.745	74.3483
3.06	76.5109	78.565	106.5683	104.0086
3.44	43.5213	55.3421	69.3742	59.1899
4.09	81.235	82.8786	74.492	76.4123
4.57	86.7889	88.487	57.6114	67.9233

First, by analyzing the model response at low TSRs, depicted in Figures 6 and 7, an overestimation of the force prediction can be noticed for the first half revolution (between 0° and 90°). However, this overestimation is lower in the ALM-SK than the one produced by the ALM-XFOIL or the vortex models. Since the operating conditions for $\lambda = 1.84$ and 2.55 correspond to the deep dynamic stall regime, a correct estimation of the force coefficients by the DSM is fundamental for the accuracy of the results. The ALM trends to simulate the drop of force in the downwind region close to 270°. In general, the shape of the force curves is well predicted by all the models, although the ALM shows an small improvement in the estimation of the force amplitude. For $\lambda = 1.84$, Table 3 reveals that the best performance is achieved by both ALM models. However, there is not a considerable difference among the performance of the models (since all the calculated standard deviation have similar value). In the case of $\lambda = 2.55$, all the models have similar prediction accuracy, besides the ALM-SK model and which has the lower value of standard deviation.

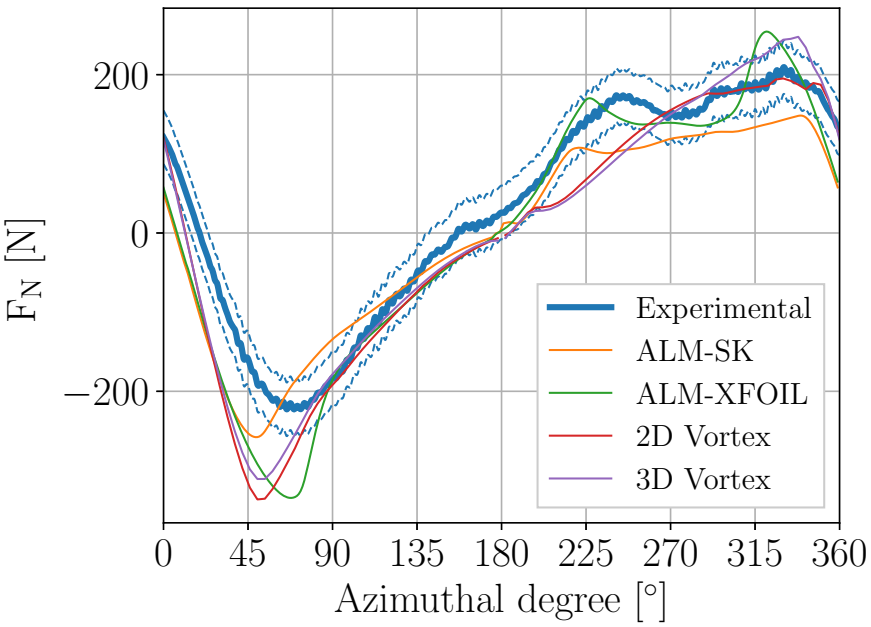

Figure 6. The normal force response at $\lambda = 1.84$.

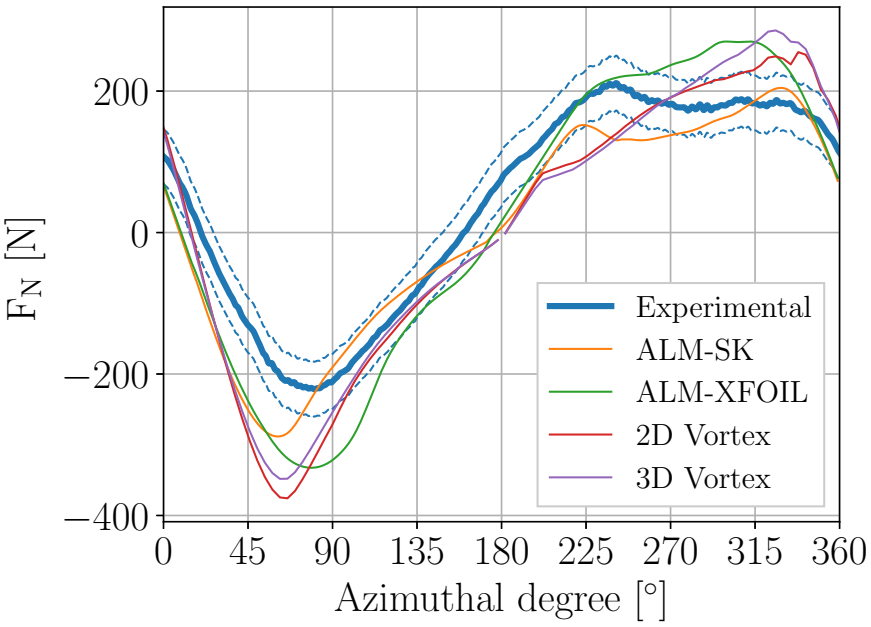

Figure 7. The normal force response at $\lambda = 2.55$.

Figure 8 shows the force response for a TSR of $\lambda = 3.06$. The trend of the simulated results is similar to the obtained ones for $\lambda = 1.84$ and 2.55, although there is an improvement in the prediction of the normal force peak in the upwind side. Regarding to the downwind side, the accuracy of the numerical results decrease in terms of the curve shape representation. All the models show good agreement with experiments. The differences between the 2D and 3D numerical results for the vortex method can be considered small. Table 3 reveals that the best performance is obtained by both ALM models.

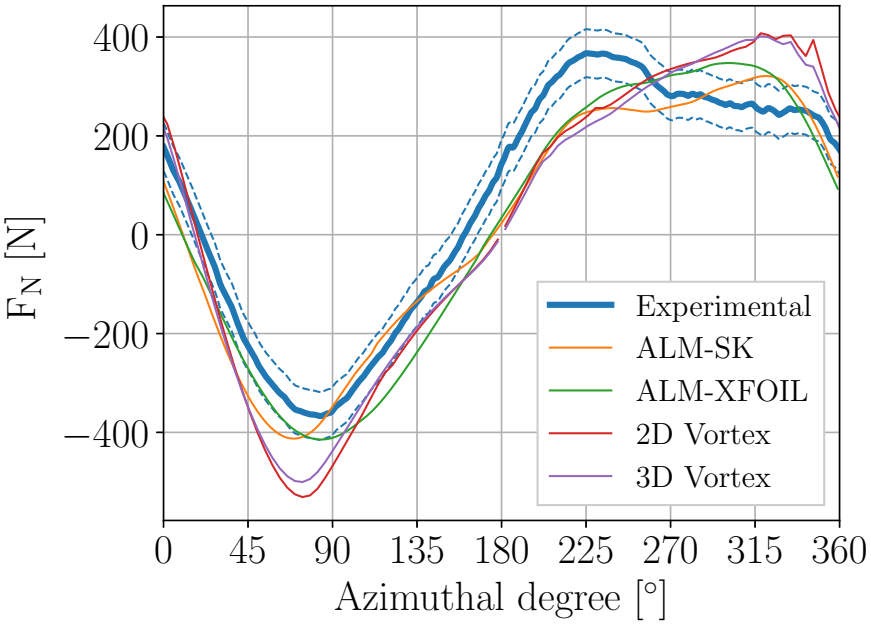

Figure 8. The normal force response at $\lambda = 3.06$.

It has to be considered when the results are inaccurate at the upwind region, it affects (disturbs) directly the accuracy on the downwind results. This can be clearly noticed in Figure 9, for the case with TSR $\lambda = 3.44$ (close to the optimal operational value), where all the models showed a satisfactory

performance. Particularly for this case, the predicted values from the ALM-SK are reasonably close to the experimental ones, where the standard deviation is the smallest one for all the presented models and tested cases. None of the models are able to represent properly the force drop in the region around 270°, which is also present in the cases for highest TSRs.

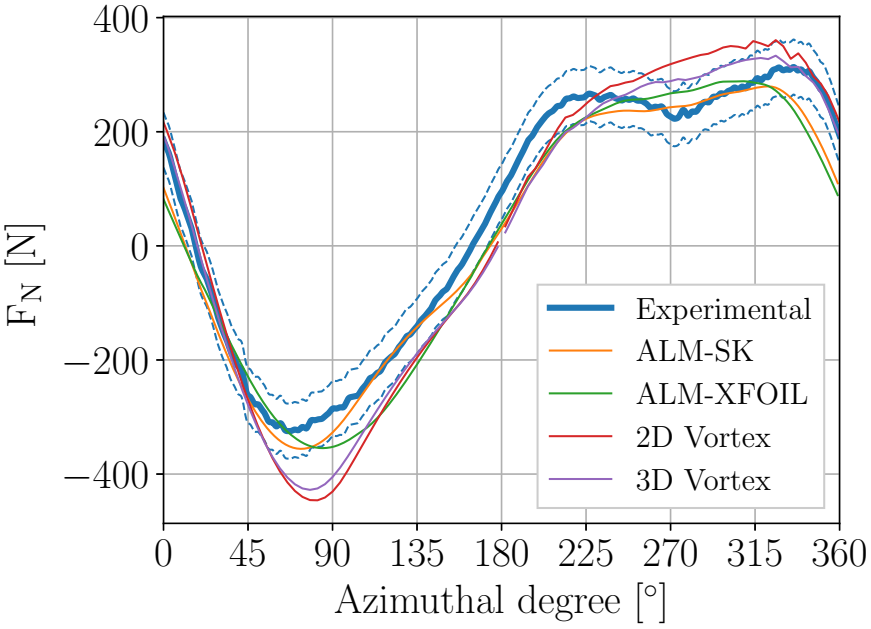

Figure 9. The normal force response at $\lambda = 3.44$.

Figures 10 and 11 depict the high TSR cases with $\lambda = 4.09$ and 4.57, respectively. All the models have good agreement with the force in the upwind section while in the downwind region there is an underestimation of the normal forces drop (which is considerably pronounced for these cases) and a noticeable lower force amplitude for the case with $\lambda = 4.57$ using the ALM. In the overall, the ALMs predict lower force amplitudes than the vortex models.

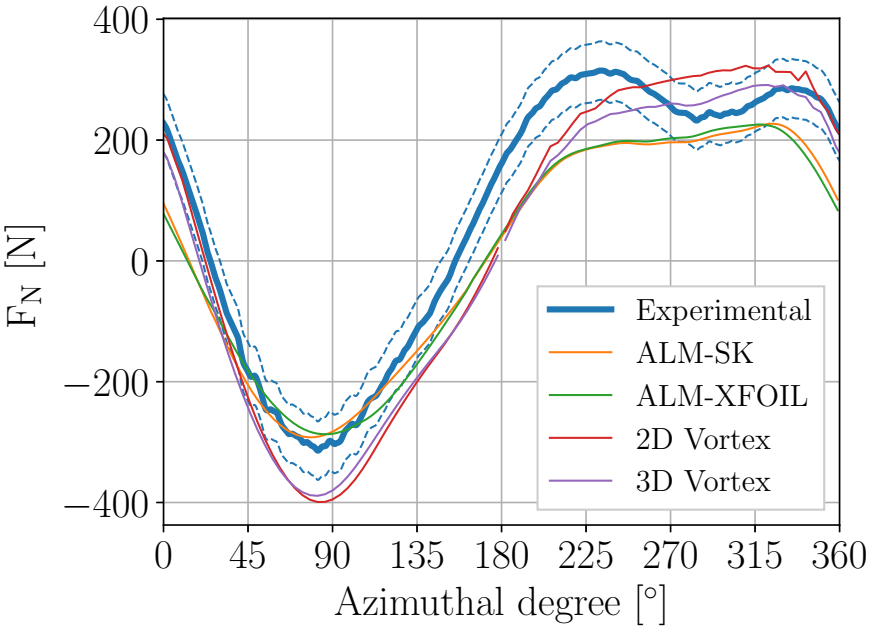

Figure 10. The normal force response at $\lambda = 4.09$.

For high TSR cases, the obtained numerical results had the less agreement with experiments in the forces magnitude description compared to the previous TSRs cases. Both ALM-SK and ALM-XFOIL have no relevant differences in their force prediction and the vortex model, in both 2D and 3D versions, performs better for these high TSRs operational conditions.

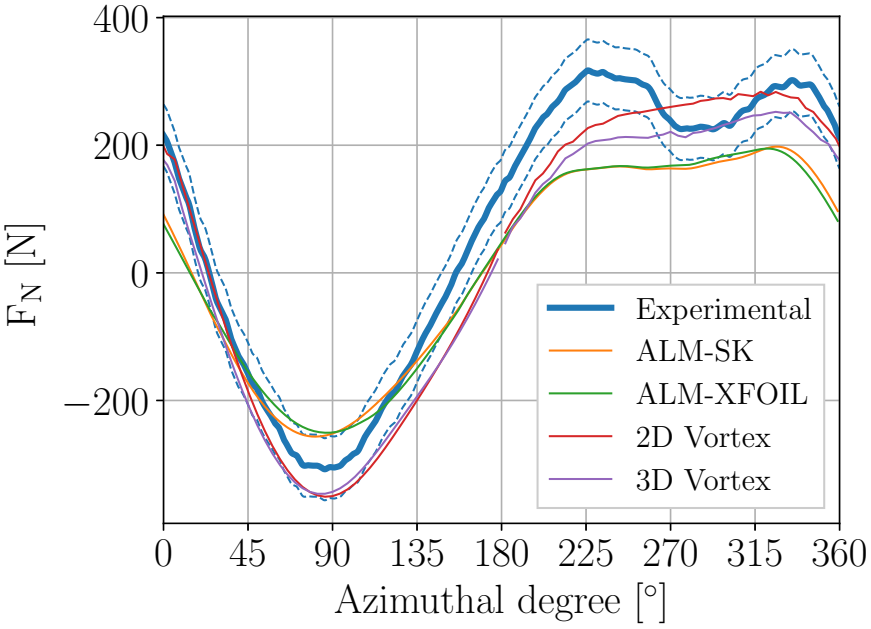

Figure 11. The normal force response at $\lambda = 4.57$.

4.4. General Discussion

A further study into the calculation of the angle of attack was carried out, showing that there is a small shift on the obtained values of around $\sim 2^\circ$ between the ALM-SK and the Vortex code. Although both models employ the same DSM and empirical data, the angle of attack calculation is one of the main differences between them, as the ALM samples the flow velocity at the blade position, while the vortex code calculates it from a potential flow solution. Therefore, the ALM, predicts larger angles of attack in the upwind section, causing the blades to go deeper into stall, giving lower power coefficient estimates. During the numerical work with, the ALM-SK model revealed that the overestimated drag force will only give a notable contribution to the C_P and not the normal force, whose main contribution comes from the lift force. Improvements of the DSM for a proper prediction of the drag coefficient C_D are required when is used together with the ALM.

For the lowest studied TSRs the 2D vortex model shows a considerable overestimation of the predicted normal force peak within the upwind side. The authors presume that this happens because the other presented models consider the three-dimensional effects which have a relevant contribution on the forces. In general, the flow should be easier to simulate for low TSRs due to the lower axial induction factor and errors there are likely due to the DSM. This is consistent with the results on Table 3, where is shown that all the models have the best performance at the low TSR of $\lambda = 1.84$.

A better performance was achieved in all the cases at the upwind side for all the models, since during the second half of the revolutions the blades are operating within the wake and therefore, the accuracy of calculated forces at the downwind side is highly dependent on the proper description of the flow field inside the rotor.

It is expected to have a similar performance for the ALM-SK and the 3D vortex model in the upwind side, since they have implemented the same DSM and moreover they use the same drag and lift coefficient. However, differences in the results likely are due to the different ways of calculating the angle of attack α: as it was mentioned the ALM uses a geometrical relation between the local sampled

inflow velocity and the blade rotational velocity, while the vortex method a potential flow solution is used.

For the experimental results at high TSRs, a pronounced force drop is present on the downwind side, which could be an effect produced from the atmospheric turbulence, hence, additional studies are needed since there is a lack on the agreement for describing this phenomenon. The relatively low computational cost has to be emphasized. If the presented work would be carried out using a three-dimensional full-body solved model, it will result in an unfeasible calculation time.

5. Conclusions

The presented models are able to reproduce the normal forces on a blade of an VAWT in an open site for a wide and diverse range of operational conditions, covering shallow to deep dynamic stall regime. In general, there is a descent agreement with experimental data in terms of the trend, magnitude and amplitude of the predicted forces. The models can be used to identify the region for the optimal TSR operation (larger obtained C_P) and maximum and minimum loads on blades within a revolution. For the simulation of the turbine power curve, there was a good qualitative representation of it for all the tested models. The ALM-XFOIL and 3D Vortex model showed better accuracy. An overestimation of the maximum available power is revealed by the 2D Vortex model, while the ALM-SK underestimates it. Improvements are required on the DSM for a proper drag coefficient estimation using the presented models. In all the studied cases for prediction of the normal forces, there was a better agreement with experiments in the upwind side compared to the downwind one. A decrease on the accuracy was present in cases with high TSRs, where there was a force drop on the second half revolution.

In general, The 2D vortex method performs as good as the 3D version of it for normal force predictions but the latter shows a considerable improvement in the reproduction of the power coefficients. Comparing the three-dimensional models (both ALMs and 3D vortex model), all of them have a good performance in all the tested cases but there was no common pattern to the disparities between the different modelling approaches. Differences can be found between them in the representation of the C_P curve, peak and drop forces in the first and second half revolution, respectively (with exception of the ALM for the higher TSRs) revealing a relevant influence by the method to obtain the angle of attack and the force coefficients data input.

Considering the performance of the models for the studied cases through the numerical results obtained, the applied ALM and vortex code can be considered as potential tools for VAWTs simulations to study the load limits at relatively low computational cost showing accuracy and stability. However, there is room for improvement. These improvements should be focused on the external sub-models employed for an appropriate force prediction: this is a whole topic of study which needs to be further developed for assuring the accuracy of models.

Author Contributions: V.M. conducted the ALM simulations. He has written the article. A.G. conducted the vortex simulations. All authors contributed to editing and reviewing of the paper. All authors have read and agreed to the published version of the manuscript.

Funding: This research received no external funding.

Acknowledgments: This work was conducted within the STandUP for Wind strategic research framework, which is part of STandUP for Energy. The computational works were performed on resources provided by the Swedish National Infrastructure for Computing (SNIC) at NSC.

Conflicts of Interest: The authors declare no conflict of interest.

References

1. Vita, L.; Paulsen, U.S.; Pedersen, T.F.; Madsen, H.A.; Rasmussen, F. Deep wind: A novel floating wind turbine concept. *Wind. Int.* **2010**, *6*, 29–31
2. Sandia National Laboratories. Offshore uSe of Vertical-Axis Wind Turbines Gets Closer Look. Available online: https://share-ng.sandia.gov/news/resources/news_releases/vawts/#.WKB9WHUrKp0 (accessed on 16 January 2018).
3. Dodd, J. First 2MW Vertiwind Vertical-Axis Prototype Built. Available online: http://www.windpowermonthly.com/article/1305428/first-2mw-vertiwind-vertical-axis-prototype-built (accessed on 16 January 2018).
4. Musgrove, P. Wind energy conversion: recent progress and future prospects. *Solar Wind Technol.* **1987**, *4*, 37–49. [CrossRef]
5. Borg, M.; Collu, M.; Brennan, F. Offshore floating vertical axis wind turbines: advantages, disadvantages, and dynamics modelling state of the art. In Proceedings of the International Conference on Marine & Offshore Renewable Energy (MORE 2012), London, UK, 26–27 September 2012.
6. Peace, S. Another approach to wind: vertical-axis turbines may avoid the limitations of today's standard propeller-like machines. *Mech. Eng.* **2004**, *126*, 28–32. [CrossRef]
7. Ribrant, J.; Bertling, L. Survey of failures in wind power systems with focus on Swedish wind power plants during 1997–2005. In Proceedings of the Power Engineering Society General Meeting, Tampa, FL, USA, 24–28 June 2007; pp. 1–8.
8. Tavner, P.; Xiang, J.; Spinato, F. Reliability analysis for wind turbines. *Wind Energy* **2007**, *10*, 1–18. [CrossRef]
9. Arabian-Hoseynabadi, H.; Oraee, H.; Tavner, P. Failure modes and effects analysis (FMEA) for wind turbines. *Int. J. Electr. Power Energy Syst.* **2010**, *32*, 817–824. [CrossRef]
10. Eriksson, S.; Solum, A.; Leijon, M.; Bernhoff, H. Simulations and experiments on a 12kW direct driven PM synchronous generator for wind power. *Renew. Energy* **2008**, *33*, 674–681. [CrossRef]
11. Sutherland, H.; Berg, D.; Ashwill, T. *A Retrospective of VAWT Technology*; Sandia Report No. SAND2012-0304; Sandia National Laboratories: Albuquerque, NM, USA, 2012.
12. Bachant, P.; Wosnik, M. Characterising the near-wake of a cross-flow turbine. *J. Turbul.* **2015**, *16*, 392–410. [CrossRef]
13. Johnston, S.J. Proceedings of the Vertical Axis Wind Turbine (VAWT) Design Technology Seminar for Industry. Available online: http://www.osti.gov/scitech/servlets/purl/6725534/ (accessed on 1 January 2019).
14. Atkins, R.E. *Measurements of Surface Pressures on an Operating Vertical-Axis Wind Turbine*; Sandia National Laboratories: Livermore, CA, USA, 1989.
15. Oler, J.; Strickland, J.H.; Im, B.; Graham, G. *Dynamic-Stall Regulation of the Darrieus Turbine*; Tech. Rep.; Department of Mechanical Engineering, Texas Tech University: Lubbock, TX, USA, 1983.
16. Strickland, J.H.; Webster, B.; Nguyen, T. A vortex model of the darrieus turbine: an analytical and experimental study. *J. Fluids Eng.* **1979**, *101*, 500–505. [CrossRef]
17. Ashuri, T.; Bussel, G.; Mieras, S. Development and validation of a computational model for design analysis of a novel marine turbine. *Wind Energy* **2013**, *16*, 77–90. [CrossRef]
18. Castelein, D.; Ragni, D.; Tescione, G.; Ferreira, C.S.; Gaunaa, M. Creating a benchmark of vertical axis wind turbines in dynamic stall for validating numerical models. In Proceedings of the 33rd Wind Energy Symposium 2015, American Institute of Aeronautics and Astronautics, 33rd AIAA/ASME Wind Energy Symposium, Kissimmee, FL, USA, 5–9 January 2015.
19. Kjellin, J.; Bülow, F.; Eriksson, S.; Deglaire, P.; Leijon, M.; Bernhoff, H. Power coefficient measurement on a 12 kW straight bladed vertical axis wind turbine. *Renew. Energy* **2011**, *36*, 3050–3053, doi:10.1016/j.renene.2011.03.031. [CrossRef]
20. Dyachuk, E.; Rossander, M.; Goude, A.; Bernhoff, H. Measurements of the aerodynamic normal forces on a 12-kW straight-bladed vertical axis wind turbine. *Energies* **2015**, *8*, 8482–8496. [CrossRef]
21. Rossander, M.; Dyachuk, E.; Apelfröjd, S.; Trolin, K.; Goude, A.; Bernhoff, H.; Eriksson, S. Evaluation of a blade force measurement system for a vertical axis wind turbine using load cells. *Energies* **2015**, *8*, 5973–5996. [CrossRef]
22. Mendoza, V.; Goude, A. Improving farm efficiency of interacting vertical-axis wind turbines through wake deflection using pitched struts. *Wind Energy* **2019**, *22*, 538–546. [CrossRef]

23. Mendoza, V.; Chaudhari, A.; Goude, A. Performance and wake comparison of horizontal and vertical axis wind turbines under varying surface roughness conditions. *Wind Energy* **2019**, *22*, 458–472. [CrossRef]
24. Mendoza, V.; Bachant, P.; Ferreira, C.; Goude, A. Near-wake flow simulation of a vertical axis turbine using an actuator line model. *Wind Energy* **2019**, *22*, 171–188. [CrossRef]
25. Mendoza, V. Aerodynamic Studies of Vertical Axis Wind Turbines Using the Actuator Line Model. Ph.D. Thesis, Acta Universitatis Upsaliensis, Uppsala, Sweden, 2018.
26. Bachant, P.; Wosnik, M. Simulating wind and marine hydrokinetic turbines with actuator lines in rans and les. In Proceedings of the APS Meeting Abstracts, San Antonio, TX, USA, 2–6 March 2015.
27. Bachant, P.; Goude, A.; Wosnik, M. Actuator line modeling of vertical-axis turbines. *arXiv* **2016**, arXiv:1605.01449.
28. Bachant, P.; Goude, A.; Wosnik, M. Turbinesfoam: v0.0.7. Available online: https://zenodo.org/record/49422#.XjOHMWYRWHs (accessed on 16 of April 2016).
29. Mendoza, V.; Bachant, P.; Wosnik, M.; Goude, A. Validation of an actuator line model coupled to a dynamic stall model for pitching motions characteristic to vertical axis turbines. *J. Phys.* **2016**, *753*, 022043. [CrossRef]
30. Mendoza, V.; Goude, A. Wake flow simulation of a vertical axis wind turbine under the influence of wind shear. *J. Phys.* **2017**, *854*, 012031. [CrossRef]
31. Sørensen, J.N.; Shen, W.Z. Computation of wind turbine wakes using combined navier-stokes/actuator-line methodology. In Proceedings of the European Wind Energy Conference EWEC 99, Nice, France, 1–5 March 1999.
32. Leishman, J.; Beddoes, T. A generalised model for airfoil unsteady aerodynamic behaviour and dynamic stall using the indicial method. In Proceedings of the 42nd Annual forum of the American Helicopter Society, Washington, DC, USA, 7–10 July 1986; pp. 243–265.
33. Sheng, W.; Galbraith, R.; Coton, F. A modified dynamic stall model for low mach numbers. *J. Solar Energy Eng.* **2008**, *130*, 031013. [CrossRef]
34. Dyachuk, E. Aerodynamics of Vertical Axis Wind Turbines: Development of Simulation Tools and Experiments. Ph.D. Thesis, Acta Universitatis Upsaliensis, Uppsala, Sweden, 2015.
35. Smagorinsky, J. General circulation experiments with the primitive equations: I. the basic experiment. *Mon. Weather Rev.* **1963**, *91*, 99–164. [CrossRef]
36. Yoshizawa, A. Subgrid-scale modeling suggested by a two-scale dia. In *Computational Wind Engineering 1*; Elsevier: Amsterdam, The Netherlands, 1993; pp. 69–76.
37. Dyachuk, E.; Goude, A. Numerical validation of a vortex model against experimentaldata on a straight-bladed vertical axis wind turbine. *Energies* **2015**, *8*, 11800–11820. [CrossRef]
38. Dyachuk, E.; Goude, A.; Berhnoff, H. Simulating Pitching Blade With Free Vortex Model Coupled with Dynamic Stall Model for Conditions of Straight Bladed Vertical Axis Turbines. *J. Solar Energy Eng.* **2015**, *137*, 041008. [CrossRef]
39. Goude, A. Fluid Mechanics of Vertical Axis Turbines: Simulations and Model Development. Ph.D. Thesis, Acta Universitatis Upsaliensis, Uppsala, Sweden, 2012.
40. Goude, A.; Rossander, M. Force measurements on a VAWT blade in parked conditions. *Energies* **2017**, *10*, 1954. [CrossRef]
41. Sheldahl, R.E.; Klimas, P.C. *Aerodynamic Characteristics of Seven Symmetrical Airfoil Sections through 180-Degree Angle of Attack for Use in Aerodynamic Analysis of Vertical Axis Wind Turbines*; Tech. Rep.; Sandia National Labs.: Albuquerque, NM, USA, 1981.
42. Drela, M. Xfoil: An analysis and design system for low reynolds number airfoils. In *Low Reynolds Number Aerodynamics*; Springer: Berlin, Germany, 1989; pp. 1–12.